Osmoregulatory inositol transporter SMIT1 modulates electrical activity by adjusting $PI(4,5)P_2$ levels

Gucan Dai[a], Haijie Yu[a], Martin Kruse[a], Alexis Traynor-Kaplan[b,c], and Bertil Hille[a,1]

[a]Department of Physiology and Biophysics, University of Washington School of Medicine, Seattle, WA 98195; [b]ATK Innovation Analytics & Discovery, North Bend, WA 98045; and [c]Division of Gastroenterology, Department of Medicine, University of Washington, Seattle, WA 98195

Contributed by Bertil Hille, April 22, 2016 (sent for review February 21, 2016; reviewed by Geoffrey W. Abbott and Donald William Hilgemann)

Myo-inositol is an important cellular osmolyte in autoregulation of cell volume and fluid balance, particularly for mammalian brain and kidney cells. We find it also regulates excitability. Myo-inositol is the precursor of phosphoinositides, key signaling lipids including phosphatidylinositol 4,5-bisphosphate [$PI(4,5)P_2$]. However, whether myo-inositol accumulation during osmoregulation affects signaling and excitability has not been fully explored. We found that overexpression of the Na^+/myo-inositol cotransporter (SMIT1) and myo-inositol supplementation enlarged intracellular $PI(4,5)P_2$ pools, modulated several $PI(4,5)P_2$-dependent ion channels including KCNQ2/3 channels, and attenuated the action potential firing of superior cervical ganglion neurons. Further experiments using the rapamycin-recruitable phosphatase Sac1 to hydrolyze PI(4)P and the P4M probe to visualize PI(4)P suggested that PI(4)P levels increased after myo-inositol supplementation with SMIT1 expression. Elevated relative levels of PIP and PIP_2 were directly confirmed using mass spectrometry. Inositol trisphosphate production and release of calcium from intracellular stores also were augmented after myo-inositol supplementation. Finally, we found that treatment with a hypertonic solution mimicked the effect we observed with SMIT1 overexpression, whereas silencing tonicity-responsive enhancer binding protein prevented these effects. These results show that ion channel function and cellular excitability are under regulation by several "physiological" manipulations that alter the $PI(4,5)P_2$ setpoint. We demonstrate a previously unrecognized linkage between extracellular osmotic changes and the electrical properties of excitable cells.

myo-inositol | ion channels | PIP_2 | phosphoinositide | SMIT1

Here we explore changes of membrane excitability that follow manipulation of the amount of intracellular myo-inositol and the cell-membrane phosphoinositide lipids that it gives rise to. Phosphoinositides, the low-abundance, informational phospholipids of cell membranes, play an important role in regulating many cellular functions (1–3). The past two decades have revealed that phosphoinositides, especially plasma-membrane localized phosphatidylinositol 4,5-bisphosphate [$PI(4,5)P_2$], are indispensable for the function of many ion channels and transporters (2, 4, 5) as well as for cellular processes such as endocytosis and release of synaptic vesicles. Cellular pools of phosphoinositides are dynamically modulated by effectors, such as phospholipase C (PLC) and PI3-kinase pathways, that respond to extracellular stimuli (1, 3). Additionally, baseline levels of phosphoinositides are adjusted by lipid kinases and lipid phosphatases (Fig. S1).

Myo-inositol, the most abundant stereoisomer of inositol in the human body, forms the head group of phosphoinositides (3). Lipid kinases and lipid phosphatases can add and remove phosphate groups at specific positions on the inositol ring, generating the eight regioisomers of phosphoinositides. Over the past 50 y, the relationship between myo-inositol and human diseases, especially mood disorders, has been investigated but still remained uncertain and debated (3). An "inositol-depletion hypothesis" was proposed to explain the finding that the common mood-stabilizing drug lithium inhibited inositol-1-monophosphatase (Fig. S1) and thereby reduced intracellular myo-inositol concentrations (6–8). However, whether lithium treats mood disorders by adjusting myo-inositol levels and impinging on the phosphoinositide signaling has been a persistent controversy (3, 9–15). Indeed, some previous literature suggested that phosphoinositide synthesis is not rate-limited by the availability of myo-inositol (14, 16).

Here we consider sodium-coupled myo-inositol transporter 1 (SMIT1). Myo-inositols are transported into the cell from the extracellular fluid by inositol transporters (3). SMIT1 is encoded by the *SLC5A3* gene on human chromosome 21 and belongs to the solute carrier 5 (SLC5) gene family (17, 18). Human SMIT1 is present in many tissues and highly expressed in brain and kidney (17, 18). It is structurally similar to glucose transporters of the same family, characterized by inverted-repeat domains and a large number of transmembrane segments (19, 20). SMIT1 has a slow substrate turnover rate of only a few per second, transporting 1 myo-inositol together with 2 Na^+ (21). The myo-inositol level in mammalian tissues ranges from 0.1 to 16 mM, depending on the tissue (22, 23). It is high in adult brain (millimolar level) and is reduced by 96% in $SLC5A3^{-/-}$ mice (24). Such mice need to be maintained on myo-inositol supplementation until weaning. Extracellular hypertonicity up-regulates expression of SMIT1, promoting the further cellular accumulation of myo-inositol. This helps to counteract hypertonic stress by increasing intracellular osmolarity. Such hypertonicity-induced increases in SMIT1 expression have been reported to require a transcription factor, tonicity-responsive enhancer binding protein (TonEBP) (25). Pathophysiological states, including chronic hypernatremia caused by renal failure or hyperglycemia associated with diabetes, can increase the osmolarity of extracellular fluids and raise intracellular

Significance

Cells living in variable environments evolve ways to adapt to altered extracellular conditions. During hypertonic stress, the expression of several human osmolyte transporters increases, thereby accumulating more osmolytes and elevating intracellular osmolarity. We focused on one of these osmolytes, myo-inositol, which is also the precursor of membrane phosphoinositide lipids. We found that intracellular accumulation of myo-inositol via its transporter SMIT1 is able to increase phosphoinositide levels and thereby modulate the activities of phosphoinositide-dependent ion channels. We provide evidence for a previously unidentified connection between the extracellular osmotic changes and the electrical properties of excitable cells. Our findings may help elucidate mechanisms underlying several diseases characterized by either perturbed myo-inositol levels or increased extracellular tonicity.

Author contributions: G.D. and B.H. designed research; G.D., H.Y., M.K., and A.T.-K. performed research; G.D., A.T.-K., and B.H. contributed new reagents/analytic tools; G.D., A.T.-K., and B.H. analyzed data; and G.D. and B.H. wrote the paper.

Reviewers: G.W.A., University of California, Irvine; and D.W.H., University of Texas Southwestern Medical Center.

The authors declare no conflict of interest.

[1]To whom correspondence should be addressed. Email: hille@uw.edu.

This article contains supporting information online at www.pnas.org/lookup/suppl/doi:10.1073/pnas.1606348113/-/DCSupplemental.

myo-inositol levels (26, 27). In addition, misregulated myo-inositol levels and/or SMIT1 dysfunction have been implicated in several devastating diseases including Down's syndrome, Alzheimer's disease, cerebral astrocytomas, multiple sclerosis, and bipolar disorder (18, 28–34). However, the underlying significance of myo-inositol and SMIT1 in these diseases remains elusive.

We find that SMIT1 overexpression and myo-inositol supplementation are able to increase intracellular phosphoinositide levels, thereby altering the phosphoinositide signaling and the electrical activities of phosphoinositide-regulated ion channels. We show that treatment with hypertonic solutions raises phosphoinositide levels and regulates cellular excitability by impinging on the TonEBP–SMIT1 pathway, suggesting complex physiological roles for SMIT1 in signaling.

Results

SMIT1 and Myo-Inositol Modulate KCNQ2/3 Channel Activity. We anticipated that elevated levels of intracellular myo-inositol would generate more phosphoinositides (refer to Fig. S1 for the synthesis of phosphoinositides from myo-inositol). The experiments focus first on functional measures of $PI(4,5)P_2$, the dominant plasma membrane phosphoinositide. KCNQ2/3 channels (K_V 7.2/7.3), which require $PI(4,5)P_2$ to be activated, served as our first readout for phosphoinositide metabolism, and G_q-coupled M_1 muscarinic acetylcholine receptors served to deplete $PI(4,5)P_2$ via activation of PLC.

The tsA201 cells were transiently transfected with KCNQ2/3 subunits and M_1 muscarinic receptors. Fig. 1*A* shows depolarizing voltage-clamp steps activating outward K^+ current (a). As has been reported many times, the current was reduced when $PI(4,5)P_2$ was depleted by applying muscarinic receptor agonist oxotremorine-M (Oxo-M) (b), and it gradually recovered after Oxo-M removal (c). The peak amplitudes of tail currents (the slow deactivating currents at −60 mV), a signature of KCNQ channels, are plotted in Fig. 1*B*. They mirror the time course of $PI(4,5)P_2$ depletion and regeneration. We anticipated an elevation of phosphoinositide pools when myo-inositol transport was augmented and predicted that the suppression of KCNQ2/3 current during application of Oxo-M would become slowed and the recovery of KCNQ2/3 current would become speeded. Channels and receptors were expressed in tsA201 cells with or without coexpression of the long-splice isoform of human SMIT1. We supplemented the culture medium with an additional 100 μM myo-inositol for overnight incubation. The final concentration of myo-inositol is within the physiological range in serum (35). The myo-inositol was never present in the bath solution during recordings. Combining SMIT1 overexpression and 100 μM myo-inositol preincubation did speed the recovery of the KCNQ2/3 channels after Oxo-M, compared with the control (Fig. 1 *B* and *C*). Henceforth we will call this treatment SMIT1/myo-inositol. Overnight 100 μM myo-inositol by itself also produced a small effect (Fig. 1*C*). Indeed, immunocytochemistry confirmed the expression of exogenous SMIT1 (Fig. 1*D*) in transfected tsA201 cells and revealed endogenous SMIT1 in untreated cells. Although the onset kinetics of current suppression were not noticeably affected by either SMIT1 or myo-inositol when the Oxo-M concentration was supermaximal (10 μM), the suppression by a low concentration of Oxo-M (0.2 μM) was greatly slowed (Fig. 1 *E* and *F*). As we will see, similar changes of channel properties in neurons have profound effects on electrical excitability and firing patterns.

Next, we depleted $PI(4,5)P_2$ with a voltage-sensitive phosphatase (VSP). The VSPs are lipid 5-phosphatases activated by large membrane depolarizations that remove the 5-phosphate from $PI(4,5)P_2$ without depleting PI(4)P and without generating IP_3 or diacylglycerol (DAG). Zebrafish VSP (Dr-VSP) and KCNQ2/3 channels were coexpressed. In Fig. 1*G*, a depolarization to −20 mV activates KCNQ2/3 outward current; a brief step

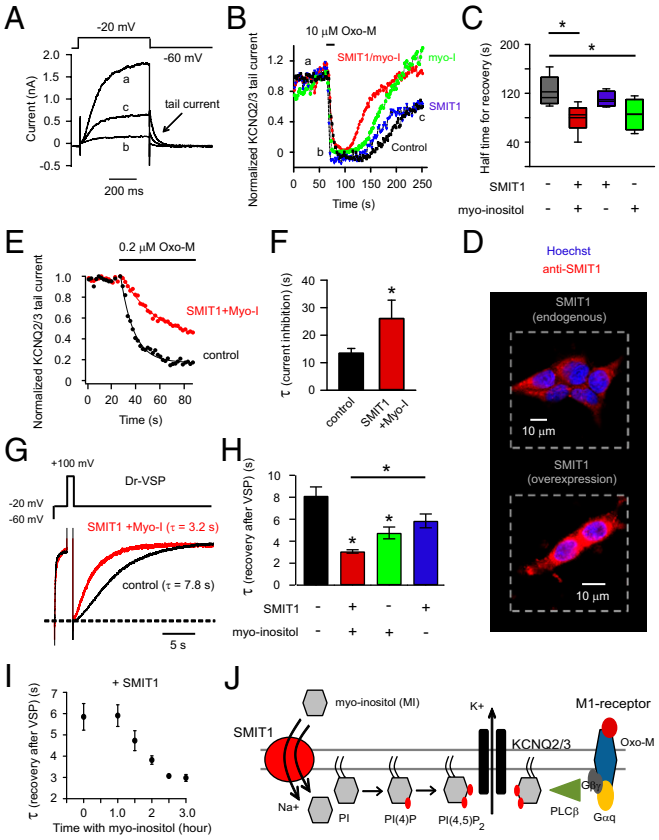

Fig. 1. Overexpression of SMIT1 and incubation with myo-inositol slow inhibition and speed recovery of KCNQ2/3 current after $PI(4,5)P_2$ depletion. (*A*) Representative current traces for KCNQ2/3 channels before (a), immediately after (b) 10 μM Oxo-M application, and during recovery (c). Arrow indicates the tail current. (*B*) Combinatorial treatments of SMIT1 overexpression with or without 100 μM myo-inositol on the KCNQ2/3 tail current recovery after M_1 receptor activation. (*C*) Summary of the data in *B*, showing the half time for current recovery (n = 4–6). (*D*) Representative confocal immunocytochemistry images showing the expression of SMIT1 protein (red) in tsA201 cells, with counterstaining for nuclei (blue). (*E*) Time courses of inhibition of KCNQ2/3 current after applying low concentrations of Oxo-M (0.2 μM), comparing control cells with cells transfected with SMIT1 plus myo-inositol. (*F*) Summary of the data in *D*, shown as the exponential time constant τ of the current inhibition (n = 4–5). *$P < 0.05$. (*G*) Current traces, showing the inhibition and recovery of KCNQ2/3 current after activation of Dr-VSP. (*H*) Summary of the data in *F*, illustrating the effects of combinatorial treatments of SMIT1 overexpression with or without 100 μM myo-inositol on the time constants of KCNQ2/3 current recovery after Dr-VSP activation (n = 4–13). Means ± SEM, *$P < 0.05$. (*I*) Effects of different durations of 100 μM myo-inositol preincubation on the τ of KCNQ2/3 current recovery after Dr-VSP activation. (*J*) Cartoon showing the hypothesis that myo-inositol entry through SMIT1 raises the intracellular levels of phosphoinositides.

to +100 mV (to activate VSP) depletes $PI(4,5)P_2$ and the channels turn off; repolarization to −20 mV allows lipid resynthesis and the channel current recovers. The recovery was faster after overnight SMIT1/myo-inositol treatment (Fig. 1 *G* and *H*). Presumably $PI(4,5)P_2$ dephosphorylation by VSP generates a larger PI(4)P pool under these conditions. Again, incubation with myo-inositol alone produced a faster recovery than the control, but the effect was less pronounced than when combined with SMIT1 overexpression (Fig. 1*H*). When SMIT1 was already overexpressed, it took about 3 h after supplementation with myo-inositol for a maximum acceleration of the KCNQ current recovery (Fig. 1*I*). This relatively long time was not surprising considering the slow turnover rate of SMIT1 for transporting myo-inositol as well as the presence of the competitive D-glucose

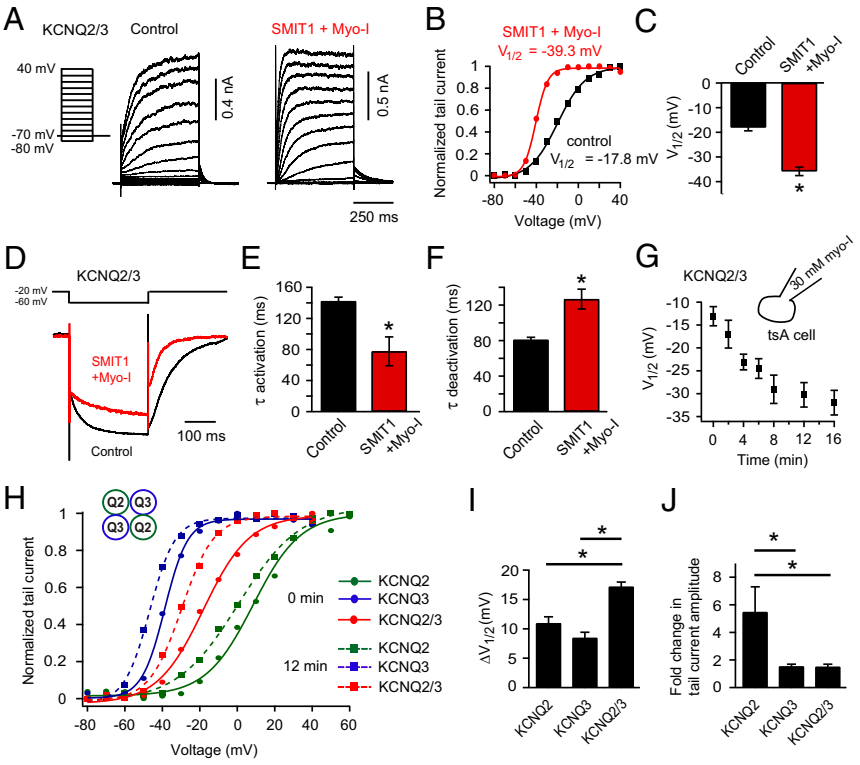

Fig. 2. SMIT1/myo-inositol enhances the voltage sensitivity of KCNQ2/3 channels. (*A*) Current traces of voltage activation of KCNQ2/3 channels with or without SMIT1/myo-inositol pretreatment, using a voltage protocol stepping from −80 mV to +40 mV. (*B*) Representative KCNQ2/3 channel conductance–voltage (G-V) relationship using the normalized tail current amplitude from *A*. (*C*) Summary of the half-maximal potential ($V_{1/2}$) in *B* for cells with SMIT1/myo-inositol compared with the control (n = 7–10). Means ± SEM, *P < 0.05. (*D*) Current traces comparing deactivation and activation of KCNQ2/3 channels with (red) or without (black) SMIT1/myo-inositol. (*E* and *F*) Summary of the time constants (τ) for deactivation and activation in *D* (n = 4–6). *P < 0.05. (*G*) Time course of the change of half-maximal potential for voltage activation ($V_{1/2}$) of KCNQ2/3 channels during dialysis of 30 mM myo-inositol in the whole-cell pipette (n = 5). (*H*) Representative G-V curves for homomeric KCNQ2, KCNQ3, and heteromeric KCNQ2+KCNQ3 channels in the beginning of the myo-inositol dialysis (0 min, circles and solid lines) compared with at 12 min during the dialysis (squares and dashed lines). (*I* and *J*) Summary of the changes of half-maximal potential ($\Delta V_{1/2}$) and the fold changes of tail current amplitudes comparing 0 and 12 min during myo-inositol dialysis for the indicated channels (n = 4–5). Means ± SEM, *P < 0.05. See also Fig. S1.

in our culture medium that should further slow the transport rate. This would also include the time for myo-inositol incorporation into lipid and reequilibration of phosphoinositide pools.

SMIT1/myo-inositol increased the voltage sensitivity of KCNQ2/3 channels. The potential for half-maximal channel activation ($V_{1/2}$) was shifted to more negative voltages (Fig. 2 *A*–*C*) and the steepness was increased. Fitting a Boltzmann equation to the conductance-voltage (G-V) curve for KCNQ2/3 channels gave slope factors of 12.2 ± 0.6 mV in the control and 6.8 ± 0.9 mV with SMIT1/myo-inositol. In addition, KCNQ2/3 channels activated faster and deactivated slower with SMIT1/myo-inositol (Fig. 2 *D*–*F*), consistent with the observed G-V curve shift. Myo-inositol could be dialyzed directly into tsA201 cells through the whole-cell recording pipette. With 30 mM myo-inositol, there was a gradual and significant leftward shift of the $V_{1/2}$ for voltage activation of heteromeric KCNQ2/3 channels. About 10 min of myo-inositol dialysis produced a saturating effect (Fig. 2*G*). Dialysis of 30 mM raffinose or sorbitol, which would increase osmolarity to the same degree as myo-inositol, served as negative controls (Fig. S2*D*). Myo-inositol produced similar shifts of $V_{1/2}$ for homomeric KCNQ2 and homomeric KCNQ3 channels, but they were less than for heteromeric KCNQ2/3 channels (Fig. 2 *H* and *I*). Homomeric KCNQ2 channels did exhibit a greater increase in current amplitude compared with homomeric KCNQ3 and heteromeric KCNQ2/3 channels (Fig. 2*J*, and also see Fig. S2 *A*–*C*). This is presumably due to a lower $PI(4,5)P_2$ affinity and lower channel open probability at normal $PI(4,5)P_2$ levels (36). Together, our results would be consistent with a direct regulation of the voltage sensitivity of KCNQ2/3 channels by $PI(4,5)P_2$. The 10-min time course suggests that this is how long it takes to augment cellular $PI(4,5)P_2$ pools after providing additional intracellular myo-inositol.

Myo-Inositol Supplementation Attenuates Action Potential Firing of Superior Cervical Ganglion Neurons. We tested the effect of myo-inositol supplementation on electrical properties of primary cultured neurons. The superior cervical ganglion (SCG) neuron has been used as a model to study native KCNQ2/3 channels, which serve as a damper on their excitability (37, 38). Neurotransmitters and drugs that close these channels remove the brake so the neurons fire more easily. However, myo-inositol, by favoring K^+ channel opening, should intensify the brake. Immunohistochemistry revealed SMIT1 expressed in SCG neurons (Fig. 3*A*), and overnight myo-inositol (100 μM) supplementation reduced action potential firing elicited by 100 pA current injections (Fig. 3 *B*–*D*). We did not observe a significant change in the input resistance (Fig. S3) or the resting membrane potential by myo-inositol. Activating endogenous M_1 receptors of untreated neurons with Oxo-M induced prolonged action potential firing, whereas supplementation with 100 μM myo-inositol shortened the period of firing (Fig. 3 *E*–*G*). To determine whether KCNQ2/3 channels were involved in these effects, we monitored the kinetics of inhibition and recovery of native M-type KCNQ2/3 current after M_1 receptor activation (Fig. 3*H*). Current recovery after applying the supramaximal concentration of Oxo-M (10 μM) was faster with myo-inositol preincubation (Fig. 3 *I* and *J*). Further, while applying a low concentration of Oxo-M (0.2 μM), the inhibition of KCNQ2/3 tail current was diminished and slowed (Fig. 3 *K* and *L*): 79 ± 3% inhibition for the control and 56 ± 8% inhibition with myo-inositol, n = 4–6, P < 0.05. These data suggest that neuronal $PI(4,5)P_2$ levels are elevated by myo-inositol supplementation, as was observed in tsA201 cells. Beside KCNQ2/3 channels, augmented regulation of other voltage-gated ion channels by an enlarged $PI(4,5)P_2$ pool might also contribute to this attenuation in action potential firing of SCG neurons. The bottom line, however, is that myo-inositol elevation reduces neuronal excitability and shortens the time window of agonist-induced increased excitability.

SMIT1/Myo-Inositol Alters $PI(4,5)P_2$ Metabolism. In addition to KCNQ2/3 channels as functional reporters of $PI(4,5)P_2$ levels, we tested the genetically expressible probes, PH-CFP and PH-YFP. Each comprises a fluorescent protein fused to the pleckstrin homology (PH) domain of PLCδ1. They bind to plasma membrane

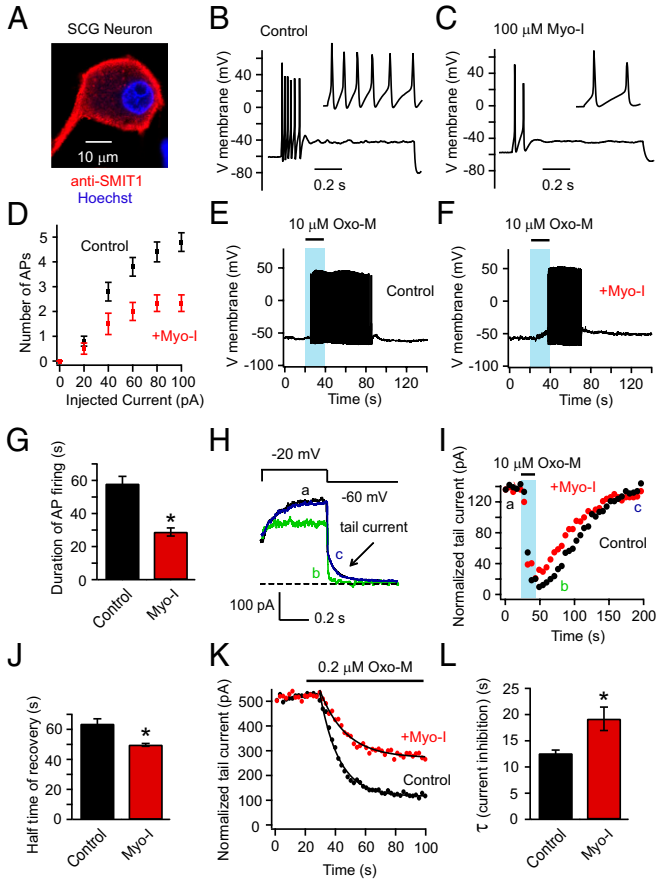

Fig. 3. Myo-inositol supplementation decreases electrical excitability of SCG neurons. (*A*) Confocal immunocytochemistry image showing endogenous expression of SMIT1 in SCG neurons. (*B* and *C*) Perforated-patch current clamp recordings showing the action potentials of SCG neurons elicited by injecting 100 pA current steps for control neurons and neurons with overnight myo-inositol supplementation. Neurons that fired tonically (about 20% of all neurons recorded) were not included. (*D*) Relationships of the number of action potentials elicited versus current injected ($n = 5$–6). (*E* and *F*) Representative action potentials of SCG neurons evoked by 20-s application of 10 μM Oxo-M. (*G*) Summary of experiments as in *E* and *F* ($n = 6$–10). Means ± SEM, $^*P < 0.05$. (*H*) Tail-current protocol for isolating the M current of SCG neurons; current traces are before (a), immediately after (b) 10 μM Oxo-M application, and after the current recovery (c). The dashed line indicates zero current. (*I*) Representative time course illustrating the effects of 100 μM myo-inositol on the recovery of tail current amplitude after M_1 receptor activation. (*J*) Summary of experiments as in *H* ($n = 5$). Means ± SEM, $^*P < 0.05$. (*K*) Time course of the inhibition of tail current after applying low concentrations of Oxo-M (0.2 μM), comparing control neurons versus neurons supplemented with myo-inositol. (*L*) Summary time constants of onset for experiments as in *K* ($n = 4$–6). Means ± SEM, $^*P < 0.05$.

$PI(4,5)P_2$. The proximity of $PI(4,5)P_2$ molecules at the membrane allows fluorescence energy transfer (Förster resonance energy transfer, or FRET) between donor CFP and acceptor YFP (Fig. 4*A*). Consistent with our previous work, when both probes were cotransfected into tsA201 cells, the FRET ratio and the KCNQ2/3 current fell in parallel during M_1 receptor activation, and both rose in parallel after agonist removal (Fig. 4*B*). As before, we found that SMIT1 plus myo-inositol speeded the recovery of the FRET ratio after Oxo-M application (Fig. 4 *C* and *D*). In separate experiments, a PH-PLCδ1-RFP probe was expressed and monitored for translocation under confocal microscopy. After M_1 receptor activation by Oxo-M, the PH-RFP probe translocated from the plasma membrane to the cytosolic region, then returned to the membrane after washout of Oxo-M (Fig. 4*E*). Again the time constant (τ) of the fluorescence recovery was shortened in cells that had been transfected with SMIT1 and treated with myo-inositol (Fig. 4 *E*, *F*, and *H*). Because PH-PLCδ1 may bind to IP_3 as well, we tested another $PI(4,5)P_2$-binding fluorescent probe with minimal IP_3-binding affinity, Tubby-YFP (39, 40). The results were similar (Fig. 4 *G* and *H*). In summary, the speeding of $PI(4,5)P_2$ recovery suggests that the pools of its precursors PI(4)P and PI might be enlarged.

SMIT1/Myo-Inositol Alters PI(4)P Metabolism. Because our experiments suggested that the $PI(4,5)P_2$ pool becomes enlarged during myo-inositol elevation, we checked whether the same might be true of PI(4)P pools. We used several strategies to study PI(4)P. First, a chemical dimerization system using rapamycin was used to deplete PI(4)P based on our previous work (Fig. 4*I*). Rapamycin can induce the dimerization of FRB and FKBP domains. In this case, FKBP is linked to an engineered PI(4)P phosphatase Sac1, and FRB to a plasma membrane anchor (41). Chemical dimerization with rapamycin translocates the enzyme from the cytoplasm to the plasma membrane. Here, FRB and FKBP were fused as well to CFP and YFP, respectively, allowing simultaneous photometric FRET-ratio measurements of enzyme translocation and patch-clamp recordings of changes of KCNQ current in the rapamycin system. Application of 5 μM rapamycin induced an abrupt and sustained increase in FRET ratio, reflecting irreversible translocation to the plasma membrane. Concurrently, the KCNQ2/3 current decreased due to the dephosphorylation of PI(4)P by Sac1 and the resulting slowing of $PI(4,5)P_2$ synthesis. We found that the inhibition of KCNQ2/3 current was significantly attenuated and the time constant of inhibition lengthened after SMIT1/myo-inositol treatment: 59 ± 5% current inhibition and τ = 55 ± 6 s for the control and only 30 ± 9% current inhibition and τ = 77 ± 4 s after SMIT1/myo-inositol ($n = 3$, $^*P < 0.05$) (Fig. 4 *J* and *K*).

Photometric FRET ratio measurements using a P4M probe (42) that specifically binds to PI(4)P were consistent with an enlarged PI(4)P pool. A high FRET ratio was generated between membrane-localized Lyn11-FRB-CFP and P4M-YFP. The FRET ratio was reduced after PI(4)P hydrolysis by applying 10 μM Oxo-M. (Fig. S4). We found the recovery of the FRET ratio was more complete with SMIT1/myo-inositol than under control conditions within the 300-s time frame after Oxo-M application (Fig. S4).

Further, the Golgi pool of PI(4)P also contributes to generation of plasma membrane $PI(4,5)P_2$ (43, 44). In contrast to the translocation of Sac1 to the plasma membrane using Lyn11-FRB, we recruited Sac1 to the trans-Golgi network using an anchored Tgn38-FRB (Fig. S5*A*) while maintaining the other features of the simultaneous photometry and electrophysiology recordings. Applying rapamycin in this situation resulted in specific hydrolysis of PI(4)P at the trans-Golgi network. We found the reduction of KCNQ current after rapamycin application was significantly blunted by SMIT1 and myo-inositol (Fig. S5). Together, these results suggest that the Golgi PI(4)P pool and/or the plasma membrane PI(4)P pool might be enlarged under these conditions.

SMIT1/Myo-Inositol Increases Phosphoinositide Levels Determined by Mass Spectrometry. So far our functional assays suggest enlarged phosphoinositide pools after intracellular myo-inositol accumulation. Do all phosphoinositide pools increase, and how much? We carried out "lipidomics" studies, for quantitative analysis of phosphoinositide species (45). Lipids were extracted from tsA201 cells with or without SMIT1/myo-inositol treatment. The extracted lipids were methylated to allow more efficient stabilization and ionization in mass spectrometry (46). The levels of phosphatidylinositol phosphate (PIP) and phosphatidylinositol bisphosphate (PIP_2) species with various aliphatic side chains were augmented two- to threefold in SMIT1/myo-inositol cells (Fig. 4 *L*–*O*). However, unexpectedly, total cellular PI seemed unchanged, suggesting that different regulatory mechanisms not related to myo-inositol

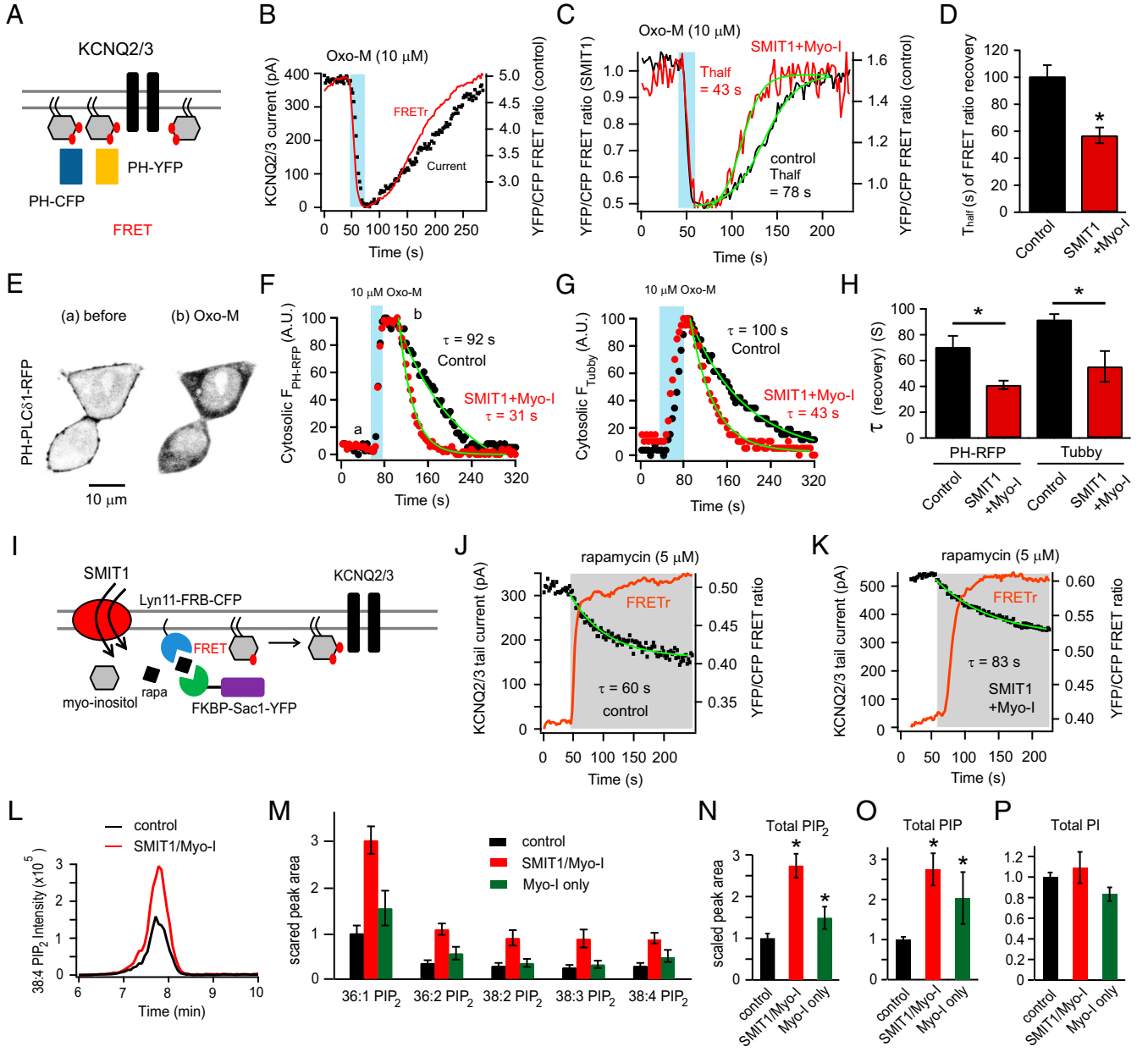

Fig. 4. SMIT1 plus myo-inositol augment PI(4)P and PI(4,5)P_2 pools. (*A*) Diagram of FRET between PH-CFP and PH-YFP, as they bind to plasma membrane PI(4,5)P_2. (*B*) Simultaneous whole-cell patch clamp recordings and photometric FRET measurements showing parallel changes of KCNQ2/3 current and the PI(4,5)P_2 pool after M_1 receptor activation by 10 μM Oxo-M. (*C*) Representative time courses of the FRET ratio after M_1 receptor activation with or without SMIT1/myo-inositol. (*D*) Summary of half time (T_{half}) of FRET ratio recovery in experiments like *C* (n = 5–6). (*E*) Confocal images showing the translocation of PH-PLCδ-RFP from the plasma membrane to the cytosol after 10 μM Oxo-M application. (*F*) Representative time courses of the normalized changes in the cytosolic PH-PLCδ-RFP fluorescence intensity after applying Oxo-M with or without SMIT1/myo-inositol; a and b correspond to the left and right images in *E*. (*G*) Similar to *F* but with Tubby-YFP instead. (*H*) Summary of exponential time constants (τ) of the recoveries of cytosolic fluorescence intensities in experiments as in *F* (n = 10–12) and *G* (n = 5–6). Means ± SEM, *P < 0.05. (*I*) Cartoon illustrating the hydrolysis of PI(4)P using a rapamycin-recruitable lipid 4 phosphatase Sac1. (*J* and *K*) Representative experiments showing the reduction of KCNQ2/3 current after applying 5 μM rapamycin with and without SMIT1/myo-inositol. (*L*) Representative mass spectrometry MRM chromatogram showing that SMIT1/myo-inositol treatment enhanced the peak intensity for C18:0/C20:4 PIP_2 extracted from tsA201 cells. (*M*) Summary histogram showing the effects of SMIT1/myo-inositol treatment on the mass spectrometry quantification of various predominant species of PIP_2 (n = 3–6). (*N–P*) Summary histograms showing the effects of myo-inositol treatment with or without SMIT1 overexpression on the mass spectrometry quantification of total PIP_2, PIP, and PI (n = 5–8). Means ± SEM, *P < 0.05.

abundance may control the overall level of that lipid (Fig. 4*P* and also see *Discussion*).

Enlarged Lipid Pools Allow More Inositol Trisphosphate Production and More Intracellular Calcium Release. Calcium signaling is important for neurons and other cells (47, 48). Inositol trisphosphate (IP_3) generation and IP_3-mediated calcium release from the endoplasmic reticulum (ER) are a key component of signaling by G_q-coupled receptors and activation of PLC. A FRET-based IP_3 indicator, LIBRAvIII, was used to monitor changes of intracellular IP_3 following activation of PLC (Fig. 5*A*) (49). The FRET ratio of this probe decreases when IP_3 levels increase. Indeed, the FRET

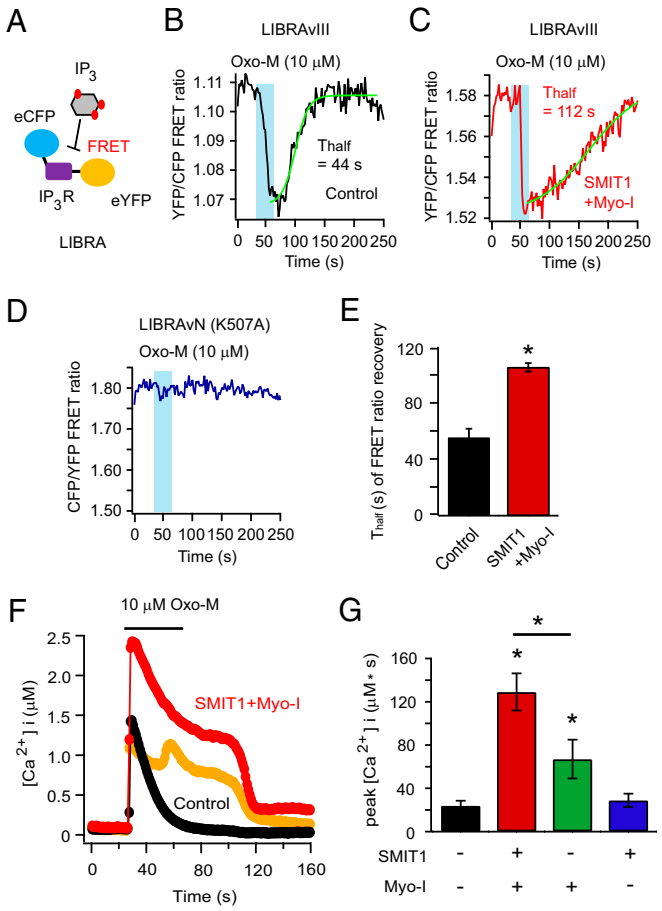

Fig. 5. SMIT1 plus myo-inositol enhances IP_3 production and calcium release from intracellular stores. (*A*) Diagram of IP_3 detection by FRET of the LIBRAvIII probe, which has a FRET pair flanking an IP_3 binding domain from the rat IP_3 receptor. (*B*) Representative control time course of the photometric FRET ratio change of LIBRAvIII induced by IP_3 generation after application of Oxo-M. (*C*) Same as *B* after SMIT1/myo-inositol treatment. (*D*) Negative control using an IP_3-insensitive LIBRA version N. The FRET ratio of LIBRAvN showed more fluctuations but was not responsive to Oxo-M. (*E*) Summary of time constants (τ) of the recoveries of LIBRA FRET ratios for experiments as in *B* and *C* ($n = 5$). (*F*) The effects of SMIT1/myo-inositol on the increase of intracellular calcium concentration after applying Oxo-M. The orange trace illustrates an example with Ca^{2+} oscillation in the same condition as the red trace. (*G*) Summary of Ca^{2+} release elicited by Oxo-M as in *F*; bars show the integral of the Ca^{2+} rise ($n = 5$–6). Means ± SEM, $^*P < 0.05$.

ratio quickly decreased when Oxo-M was applied and then recovered after agonist removal, mainly due to the hydrolysis of IP_3 by IP_3-5-phosphatase (50). If an augmented $PI(4,5)P_2$ pool is hydrolyzed, more IP_3 would be generated and the recovery of the FRET ratio would take longer. As anticipated, the recovery of the LIBRAvIII FRET ratio was delayed after SMIT1/myo-inositol treatment (Fig. 5 *B* and *C*). A mutant version of the probe, (K507A) LIBRAvN, without the IP_3 binding abilities served as a negative control (Fig. 5*D*).

Next, we tested whether the augmentation of IP_3 production after SMIT1/myo-inositol treatment induced a larger calcium release. We used the low-affinity ratiometric calcium indicator Fura4F to measure calcium dynamics after M_1 receptor activation (*SI Experimental Procedures*). Application of Oxo-M for 40 s elicited a modest calcium peak in M_1R-expressing control cells. SMIT1/myo-inositol treatment dramatically enhanced the calcium elevation: The intracellular calcium rise was more prolonged and exhibited oscillatory features (Fig. 5 *F* and *G*). Preincubation with myo-inositol alone also increased the calcium peak but to a lesser extent (Fig. 5*G*). A similar myo-inositol–mediated augmentation of calcium release was also observed with a shorter (5 s) application of Oxo-M.

SMIT1/Myo-Inositol Modulates Other $PI(4,5)P_2$-Dependent Channels: GIRK2 and TRPM7. Are the effects of myo-inositol elevation seen more generally on other components of neuronal excitability? We tested the effects of SMIT1/myo-inositol on two $PI(4,5)P_2$-dependent ion channels that are structurally distinct from KCNQ. The G protein coupled inward rectifier potassium channel GIRK2 requires $PI(4,5)P_2$ and Gβγ subunits for activity (51, 52). GIRK2 was coexpressed with the $G_{i/o}$-coupled M_2 muscarinic receptor and Dr-VSP. Applying 10 μM Oxo-M in the presence of high extracellular potassium (90 mM KCl) elicited an inward K^+ current within ∼4 s (Fig. 6 *A* and *C*). The current sagged toward a quasi-steady state (53). A large 1-s depolarizing voltage pulse (+100 mV) was applied to activate VSP and deplete $PI(4,5)P_2$. Afterward the GIRK2 current induced by M_2 receptor activation was gone, but soon it recovered as $PI(4,5)P_2$ was resynthesized. Compared with control cells, the speed of this recovery was faster after SMIT1/myo-inositol (Fig. 6 *A*, *B*, and *D*; also see coexpression of SMIT1 with M_1 and M_2 receptor together in Fig. S6).

We also tested the effects of SMIT1/myo-inositol on a transient receptor potential channel TRPM7 that depends on $PI(4,5)P_2$ (54). Compared with control cells coexpressing M_1 receptors and TRPM7 channels, we found that inhibition of the TRPM7 current was significantly delayed by SMIT1/myo-inositol (Fig. 6 *E*–*G*). Thus, the dynamics of both GIRK2 and TRPM7 channels and hence cellular excitability are significantly changed as a consequence of raising intracellular myo-inositol.

Hypertonicity Increases Phosphoinositide Levels and Regulates Cellular Excitability by Activating the TonEBP–SMIT1 Pathway. Hypertonicity suffices to induce increased SMIT1 expression in several cell types (55, 56). This is considered adaptive because the transporter will import more myo-inositol as an osmolyte that compensates for the raised extracellular solute. A proposed pathway for the increased expression of several transporters involves activation of AKAP13 (Brx), p38 MAP kinase, and the transcription factor, tonicity-responsive enhancer binding protein (TonEBP or NFAT5) (Fig. 7*N*) (25, 56–58). Activated TonEBP binds to the enhancer region of the *SLC5A3* gene, stimulating transcription (25, 58). For tsA201 cells, we added 150 mOsm raffinose to the culture medium along with 100 μM myo-inositol to produce a hypertonic environment. Protein levels of endogenous SMIT1 increased about fourfold after overnight exposure to hypertonicity (Fig. 7*A*). In parallel, KCNQ2/3 current recovery after current inhibition by VSP was accelerated (Fig. 7 *B* and *C*). In contrast, KCNQ2/3 current recovery was slowed when the endogenous SMIT1 was knocked down using an siRNA against SMIT1 (Fig. 7 *A*–*C*). Further, the voltage sensitivity of KCNQ2/3 channels was left-shifted by overnight hypertonicity (Fig. 7 *D*–*F*). KCNQ2/3 channels activated faster and deactivated slower in response to voltage changes after hypertonicity (Fig. 7*D*). Moreover, silencing the transcription factor TonEBP using a specific siRNA abolished the increase of voltage sensitivity for KCNQ2/3 channels after hypertonic stress (Fig. 7 *E* and *F*). Additionally, overnight hypertonicity reduced action potential firing in SCG neurons (Fig. 7 *G* and *H*).

There were many additional parallels between the results of hypertonic treatment and those of SMIT1/myo-inositol. Hypertonic treatment speeded return of the PH-PLCδ1-RFP probe to the plasma membrane after Oxo-M; a proteasome inhibitor MG-132, which attenuates the translocation of TonEBP from the cytosolic region to the nucleus (59, 60), diminished this effect (Fig. 7 *I* and *J*). Similarly, siRNA against TonEBP prevented the

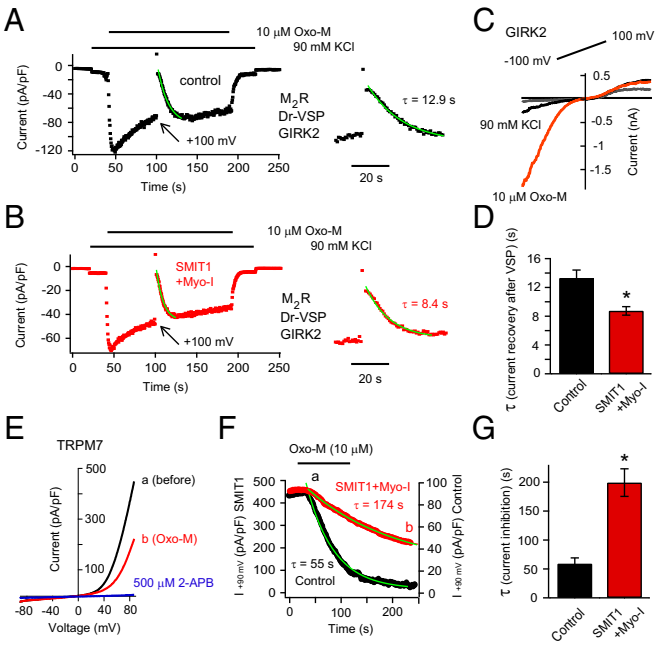

Fig. 6. SMIT1/myo-inositol regulates GIRK2 and TRPM7 channels. (*A*) Representative time course for currents at −90 mV of GIRK2 channels coexpressed with M_2 muscarinic receptors and Dr-VSP. (*Inset*) An expanded view. (*B*) GIRK2 current time course similar to *A*, but after SMIT1/myo-inositol. (*C*) GIRK2 current elicited by a voltage ramp from −100 mV to +100 mV before and after applying 10 mM Oxo-M. (*D*) Summary of the effects of SMIT1/myo-inositol on the τ of the current recovery after VSP activation in experiments like *A* and *B* (n = 7–9). (*E*) TRPM7 current traces elicited by a voltage ramp from −90 mV to +90 mV. Outward TRPM7 currents were reduced by Oxo-M application (a) and almost fully inhibited by 500 μM 2-APB (b). (*F*) Time course of the current decay of TRPM7 channels induced by Oxo-M application for the control and SMIT1/myo-inositol cells. a and b correspond to the traces shown in *E*. (*G*) Summary of the effects of SMIT1/Myo-inositol on the τ of the TRPM7 current decay after Oxo-M application in experiments like *F* (n = 4–5). Means ± SEM, $^*P < 0.05$.

effect of hypertonic stress. Experiments using mass spectrometry confirmed that hypertonicity together with myo-inositol supplementation enlarged PIP and PIP_2 pools (Fig. 7*K*). Moreover, hypertonicity augmented the IP_3-mediated calcium release, and treatments with MG-132 and siRNA against TonEBP attenuated this effect (Fig. 7 *L* and *M*). Thus, by increasing the cellular accumulation of myo-inositol through the TonEBP/SMIT1 pathway, hypertonicity not only protects against osmotic damage but at the same time modulates ion channel activities, intracellular calcium signaling, and cellular excitability (Fig. 7*N*).

Discussion

We found that elevating intracellular myo-inositol increases polyphosphoinositide levels and modulates neuronal activities via $PI(4,5)P_2$-dependent ion channels. In the opposite direction, lowering SMIT1 expression by siRNA reduces $PI(4,5)P_2$. Our findings, which we have confirmed by multiple approaches, may help elucidate mechanisms underlying several diseases characterized by perturbed myo-inositol levels or by increased extracellular tonicity.

To our surprise, the mass spectrometry experiments did not detect a significant increase in total PI levels. This result seems consistent with previous findings that SMIT1 knockout mice ($SLC5A3^{-/-}$) did not exhibit significant loss in PI even though their myo-inositol levels were greatly reduced (14, 24). There, myo-inositol supplementation was required to avoid an otherwise lethal knockout phenotype. Perhaps because no change of total PI had been seen in these mice the levels of $PI(4,5)P_2$ and PI(4)P were supposed to be invariant and were not further investigated (24). A large proportion of total PI is located in intracellular organelles, such as the ER (1, 61). Thus, our mass spectrometry of control cells estimated that total PI in tsA201 cells is 15 ± 1-fold higher than total PIP and 25 ± 2-fold higher than total PIP_2 (n = 5), as is typical of other eukaryotic cells and making PI the easiest phosphoinositide to measure. Perhaps the majority of this PI is in pools regulated by regulatory mechanisms that are not very sensitive to the availability of myo-inositol. At the same time, in the SMIT1 transfected cells, the speeding of PI(4)P and $PI(4,5)P_2$ recovery after M_1 receptor activation and the considerable enlargement of the total PIP and PIP_2 pools might be best explained if there were some minor PI pool, for example at the plasma membrane (PM), that was sensitive to myo-inositol levels and became significantly enlarged. This hypothetical local pool would have to be small enough not to make an appreciable contribution to the total cellular PI that we measured but still able to serve as the precusor for the polyphosphoinositides. Previous work in hepatocytes found that the rate of [^{3}H]myo-inositol incorporation into PI increased sevenfold when the extracellular myo-inositol concentration (30-min incubation) was elevated from 10 μM to 100 μM (9). This faster incorporation shows that some cellular pool of PI responds rapidly to ambient myo-inositol. Further biochemical work combining radiolabeled myo-inositol tracers and mass measurements could provide more information to test our hypothesis.

A recent study reported that SMIT1 and KCNQ1 channels with the auxiliary channel subunit KCNE2 show a reciprocal regulation in the brain, suggested to be due to formation of direct channel–transporter complexes (35). Our findings do not exclude such channel–transporter complexes for KCNQ2/3. However, we think the SMIT1 effects on KCNQ2/3 and several other channels that we have reported have a more general explanation, the elevation of phosphoinositide levels. In addition, we found that the voltage sensitivity of KCNQ2/3 channels became enhanced. This was not found for KCNQ1 or KCNQ1+KCNE2 channels using similar treatments (35). Reminiscent of the previous research using overexpression of PI(4)P-5 kinase to increase $PI(4,5)P_2$ levels (62–64), here we confirmed that the voltage sensitivity of KCNQ2/3 can be regulated by manipulating $PI(4,5)P_2$ levels. Consistent with the KCNQ1 data (35), we did observe an enhancement of the amplitude of KCNQ2/3 current after myo-inositol supplementation. Moreover, along with the previous finding that moderate changes of $PI(4,5)P_2$ levels affect only KCNQ2/3 current amplitude but not voltage sensitivity (65), our findings suggest that the enhancement of voltage sensitivity for KCNQ2/3 channels is revealed only when the $PI(4,5)P_2$ pool is increased on a large scale. In response to an initial elevation in membrane PIP_2 levels, the channel open probability increases, but as the open probability saturates, the channels can start to exhibit enhanced voltage sensitivity if the PIP_2 level is increased further.

Regulation by cell volume of cellular excitability via ion channels has been investigated recently (66–70). These studies focused on swelling-activated ionic conductances, including activation of several chloride and potassium channels by hypotonicity, and also regulation of TRP channels by hypertonicity (71, 72). These changes in channel activities are usually fast and reversible, presumably achieved by directly altering the channel gating with structural perturbations induced by the cell volume changes. Particularly, KCNQ1 and KCNQ4 channels, but not KCNQ2/3 channels, can sense small changes in cell volume via interactions between their cytoplasmic domains and the cytoskeleton (70). In contrast, we find that hypertonicity can regulate channel activities via transporter gene expression, myo-inositol accumulation, and enzymatic reactions, which therefore take longer time and are more sustained. Inhibition of the transcription factor TonEBP can reverse the effect, implicating the canonical TonEBP–osmolyte transporter pathway in this regulation (57). Additionally, the

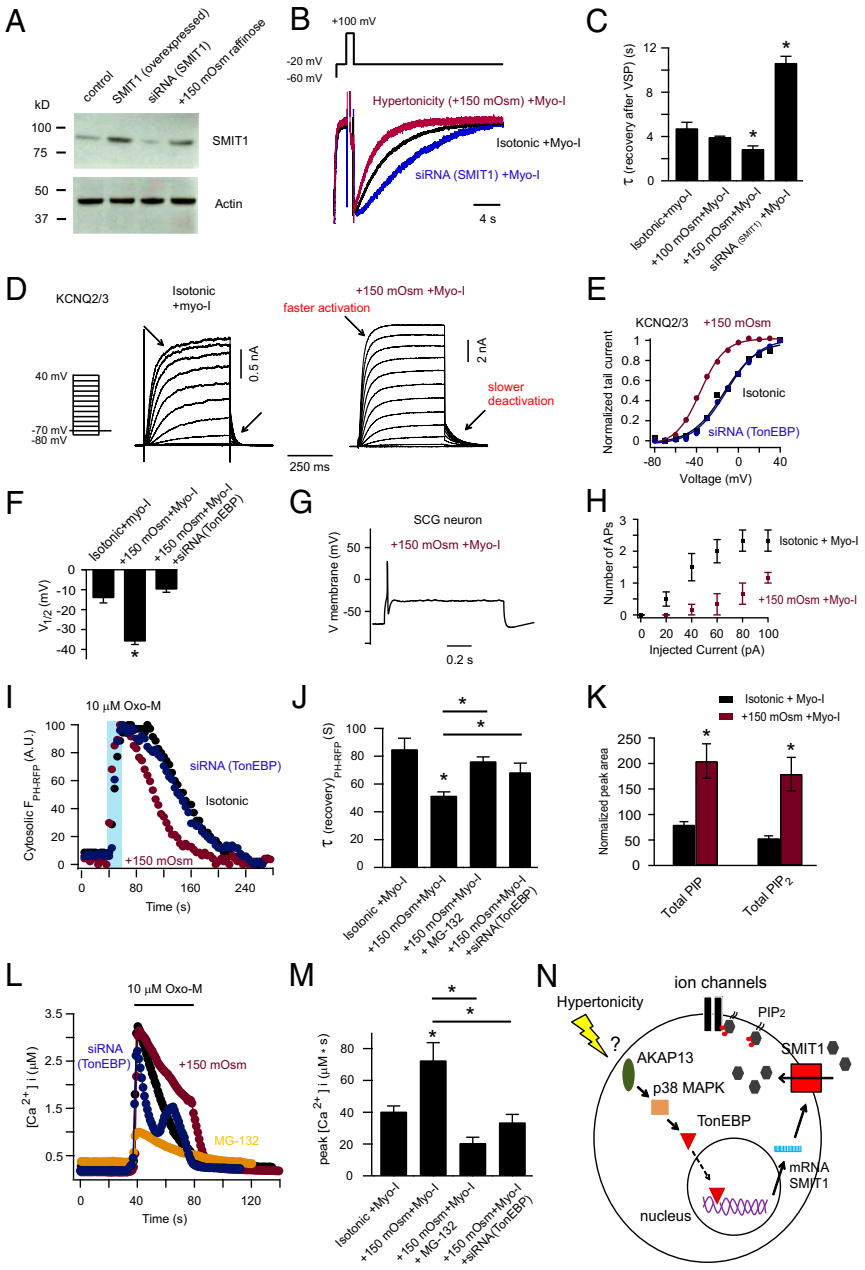

Fig. 7. Hypertonicity activates the TonEBP-SMIT1–PI(4,5)P_2–KCNQ channel pathway. (*A*) Western blot showing that 24-h hypertonic (+150 mOsm raffinose) treatment increased SMIT1 expression, whereas siRNA against SMIT1 decreased endogenous SMIT1 expression. See *SI Experimental Procedures*. (*B*) Hypertonicity (+150 mOsm raffinose) increased the speed of recovery after suppression of KCNQ2/3 current by Dr-VSP, whereas siRNA against SMIT1 produced the opposite effect. The same VSP protocol was used as in Fig. 1*G*. (*C*) Summary of recovery time constants from *B* (n = 4–13). Means ± SEM, $^*P < 0.05$. (*D*) Representative current traces of voltage activation of KCNQ2/3 channels for control cells and after hypertonic treatment. (*E*) KCNQ2/3 channel G-V relationship for control cells and after hypertonic treatment with or without transfection of siRNA against TonEBP. (*F*) Summary of the $K_{1/2}$ changes in *E*. (*G* and *H*) Hypertonicity treatment reduced the action potential firing of SCG neurons (n = 6). (*I*) Hypertonicity treatment accelerated the return of PH-RFP to the plasma membrane after depletion of PI(4,5)P_2 by M_1 receptor activation, whereas siRNA against TonEBP prevented the effect induced by hypertonicity. (*J*) Summary showing the effect of hypertonicity on the translocation of PH-RFP after PI(4,5)P_2 depletion in *I*; proteasome inhibitor MG-132 and TonEBP siRNA partially removed the effect; n = 7–13, $^*P < 0.05$. (*K*) Increase of PIP and PIP_2 levels by hypertonicity treatment measured by mass spectrometry (n = 3). (*L*) Twenty-four–hour hypertonicity (+150 mOsm raffinose) treatment increased the IP_3-mediated calcium release, whereas MG-132 treatment and siRNA against SMIT1 prevented the effect. (*M*) Summary of calcium measurements in *L* (n = 4–22, $^*P < 0.05$). (*N*) Cartoon diagram illustrating the inferred pathway for hypertonicity to regulate cellular excitability by elevating phosphoinositide levels.

phenomena we describe differ at least in part from the fast (minutes) and reversible enhancement of lipid kinase activities also induced by hypertonicity (73, 74). Considering the nearly ubiquitous expression of TonEBP (25, 75), our findings should have very broad physiological significance on cell signaling and responsiveness.

Experimental Procedures

DNA Constructs. The sources of cDNA plasmids are as follows: SMIT1 from Geoffrey W. Abbott, University of California, Irvine; untagged and eYFP-labeled mouse M_1 receptor (M_1R and M_1R-YFP) from Neil M. Nathanson, University of Washington, Seattle; human KCNQ2 from David McKinnon, State University of New York, Stony Brook, NY; human KCNQ3 fromThomas J. Jentsch, Leibniz-Institut fur Molekulare Pharmakologie, Berlin; eCFP-PH(PLCδ1) and eYFP-PH(PLCδ1) from Kees Jalink, The Netherlands Cancer Institute, Amsterdam; the zebrafish voltage-sensitive phosphatase Dr-VSP-IRES-GFP (Dr-VSP) from Yasushi Okamura, Osaka University, Osaka; LIBRAvIII and LIBRA vN from Akihiko Tanimura, Health Sciences University of Hokkaido, Tobetsu, Japan; Tubby and P4M-YFP from Tamas Balla, NIH, Bethesda and modified by M.K.; and GIRK2 and M_2 receptor from Nathan Dascal, Tel Aviv University, Tel Aviv. Membrane-targeted Lyn11-FRB-CFP, Golgi-targeted Tgn38-FRB-CFP, and YFP-FKBP-Sac1 were provided by Tamas Balla (NIH); Gerald R. Hammond, University of Pittsburgh, Pittsburgh; and Takanari Inoue, Johns Hopkins University, Baltimore. TRPM7-expressing HEK293 cells were provided by Andrew M. Scharenberg, Seattle Children's Hospital, Seattle.

Cell Culture. TsA201 cells or HEK293 cells stably expressing tetracycline-inducible human TRPM7 channels were cultured in DMEM (Gibco 11995, which contains 40 μM myo-inositol) with 10% serum and 0.2% penicillin/streptomycin. Cells were cultured in a 5% CO_2-humidified environment at 37 °C. Cells were transfected at 75–90% confluency in a 35-mm Petri dish with 0.4–1.5 μg of DNA or 7 μL of 10 μM siRNA using Lipofectamine 3000 (Invitrogen) and plated on poly-D-lysine coated glass cover-slip chips (#0; Thomas Scientific) the day preceding the experiments. The time between transfection and experiments was 24–48 h. For expression of TRPM7 channels, 1 μg/mL tetracycline was added to the media around 7 h after plating the cells on glass chips. Sprague-Dawley rats were handled and killed according to guidelines

approved by the University of Washington Institutional Animal Care and Use Committee. The rat SCG neurons were prepared and cultured for 1–2 d as described previously (76).

Electrophysiology. Whole-cell patch-clamp recordings were performed with an EPC9 patch-clamp amplifier and Patchmaster 2.35 (HEKA) at a sampling rate of 10 kHz. Borosilicate patch electrodes were made using a P97 micropipette puller (Sutter Instrument), generating an initial pipette resistance of around 3 MΩ. Recordings were made at 22–24 °C. For perforated whole-cell patch-clamp experiments, we used 0.5 mg/mL amphotericin B in the pipette solution.

For the voltage activation of KCNQ channels, the channel conductance–voltage relationship was fitted with a Boltzmann equation:

$$I = I_{min} + (I_{max} - I_{min})/(1 + \exp[(V_{1/2} - V_m)/k]),$$

where I_{max} is the maximum tail current at –70 mV after strong depolarization, I_{min} is the minimum tail current after hyperpolarization, V_m is the test pulse membrane potential, $V_{1/2}$ is the potential for half-maximal activation, and k is the slope factor.

Photometric FRET Measurement. We used an epifluorescence photometry system to measure FRET similar to the previous work in our laboratory (77). The excitation wavelength was scanned from 300 to 500 nm in 200 ms (440 nm for CFP and 500 nm for YFP using a three-color dichroic mirror). Emission of 460–480 nm was collected for CFP emission, and a 30-nm window around 535 nm was collected for YFP emission. FRET ratio was calculated using the equation FRET ratio = YFP_{CFP}/CFP_{CFP}. For YFP_{CFP} and CFP_{CFP}, the first three letters indicate the emitting fluorophore and the subscript indicates the excitation wavelength. The YFP_{CFP} was corrected by subtracting 0.79*CFP_{CFP} and 0.07*YFP_{YFP} from the raw YFP_{CFP} intensity. 0.79*CFP_{CFP} is the calibrated bleed-through of CFP emission at the YFP emission wavelength and 0.07*YFP_{YFP} is the cross-talk of direct excitation of YFP by CFP excitation. Our FRET ratios report the dynamics of FRET changes but do not give the absolute FRET efficiency.

Lipid Extraction. Cells with high confluency (1–3 million cells) on 35-mm culture dishes were gently washed twice with Ringer's Solution (2 × 1 mL). Then 1 mL of ice-cold Ringer's solution was added to resuspend cells from each dish. Subsequently, cells were centrifuged in a 1.5-mL Eppendorf tube at 12,000 × *g* for 3 min at 4 °C and then resuspended in 40 μL ice-cold double-distilled H_2O (ddH_2O) with trituration of 10 times; 10–15 μL of 6 N HCl and 100 μL of l-butanol was added to the cell pellet mixture, vortexed vigorously, and allowed to sit on ice for 10 min followed by centrifugation for 2.5 min at 12,050 × *g* and 4 °C. The upper butanol phase was transferred to a new tube. An additional 100 μL of l-butanol was added to the aqueous phase followed by vortexing and centrifugation for 2.5 min at 12,050 × *g*, after which the 100 μL butanol phase was combined with the butanol phase from the first extraction. One hundred microliters of chloroform was added to the aqueous phase followed by vortexing and centrifugation for 2.5 min at 12,050 × *g*. The lower chloroform phase was combined with the butanol extracts. This was followed by two additional chloroform wash steps as described above. The samples were then taken to dryness under N_2 before derivatization. Ninety microliters of methanol/CH_2Cl_2 4/5 vol/vol was added to the sample followed by 20 μL of 2 M TMS-diazomethane (Sigma-Aldrich). The mixture was incubated at room temperature for 1 h before being applied to ultra performance liquid chromatography (UPLC) coupled mass spectrometry.

Mass Spectrometry. The butanol-extracted lipid samples were dried under N_2, resuspended in 90 μL methanol/ dichloromethane, and derivatized with trimethylsilyldiazomethane for injection on a UPLC coupled Xevo TQ-S triple quadrupole mass spectrometer (Waters Corp.). Two- to five-microliter derivitized samples were injected into the port of a C4 column (Waters Acquity UPLC Protein BEH C4, 300A, 1.1 × 100, 1.7 μm). The mobile phase consisted of a gradient initiated with 10 mM formic acid in water (A) and 10 mM formic acid in acetonitrile (B) (50:50 vol/vol) delivered at a flow rate of 0.1 mL/min. The gradient progressed to 85% B from 1 to 10 min following injection. For determinations of exact mass, the effluent was monitored by a Waters Micromass Synapt Ion Mobility TOF/MS/ion-mobility spectrometry/MS. For quantitative analysis the effluent was monitored in a multiple reaction monitoring (MRM) mode with postcolumn infusion of 50 μM Na formate at 5 μL/min. Peak areas of individual lipid species were quantified using Waters Quanlinks software. Peak areas were normalized to PIP_2 and PIP internal standards (C17:0, C20:4; Avanti Polar Lipids) and further corrected to protein amounts using bicinchoninic acid (BCA) protein assays (Thermo Scientific).

Calcium Imaging. Intracellular calcium concentration ($[Ca^{2+}]_i$) was measured with a low-affinity calcium dye Fura4F (Invitrogen). Membrane-permeable Fura-4F-AM ester was diluted to 2 μM in Ringer's solution together with 0.2% pluoronic F-68. At room temperature, tsA201 cells were treated for 15 min with the Fura-4F-AM containing Ringer's solution and then pre-incubated in normal Ringer's for an additional 30 min for deesterification by cellular endogenous esterases. Calcium imaging used an inverted microscope (TE2000-U; Nikon) equipped with a polychrome monochromator (TILL Photonics) and an Evolve CCD camera (Photometrics). Every 1 s, Fura-4F was excited with an alternation of light sources between 340-nm and 380-nm wavelengths, and the emission fluorescence was measured at 510 nm. Metafluor fluorescence ratio imaging software (Molecular Devices) was used for collecting, displaying, and analyzing the imaging data. The ratiometric calculations took the ratio of emissions at two excitation wavelengths (R = ratio F_{340}/F_{380}) in selected cytosolic regions of individual cells. Background fluorescence was subtracted for every cell. To determine calcium concentration we used the equation $[Ca^{2+}]_i = K'(R - R_{min})/(R_{max} - R)$. K′ was calculated after the calibration of our calcium imaging system with the equation $[Ca^{2+}]_i = K'(R_{mid} - R_{min})/(R_{max} - R_{mid})$. R_{max} was obtained by applying 15 μM ionomycin in an extracellular Ringer's solution containing 10 mM Ca^{2+}. R_{min} was obtained by applying 1 μM thapsigargin and 10 μM CCCP to deplete the calcium from the intracellular stores as well as applying high concentrations of calcium chelators (10 mM EGTA) and 15 μM ionomycin in the bath. R_{mid} was obtained similarly to R_{min}, but using 10 mM HEDTA buffer titrated with $CaCl_2$ to 2 μM free-calcium concentration following the online WEBMAXC (STANDARD) calculator. The resulting values for Fura4F for K′, R_{max}, and R_{min} were 41.1 μM, 14.16, and 0.43, respectively. Solutions were exchanged by a local perfusion system that allowed complete exchange of extracellular solutions within 0.5 s. All of the measurements were done at room temperature (22–24 °C).

Data Analysis. Data parameters were expressed as mean ± SEM of *n* experiments unless otherwise indicated. Statistical significance was determined by using two-tailed Student's *t* test.

For immunocytochemistry and Western blot see *SI Experimental Procedures*.

ACKNOWLEDGMENTS. We thank Drs. Duk-Su Koh, Seung-Ryoung Jung, Jong Bae Seo, Eamonn J. Dickson, and Oscar Vivas for advice and assistance with electrophysiology, confocal microscopy, immunocytochemistry, calcium imaging, and mass spectrometry; Dr. Dale Whittington and the Mass Spectrometry Center of the School of Pharmacy for help with mass spectrometry; Dr. Geoffrey W. Abbott for advice and sharing SMIT1 cDNA; Dr. Sharona E. Gordon for advice and sharing laboratory equipment and chemicals; Drs. Duk-Su Koh, Michael D. Varnum, William N. Zagotta, and David E. Clapham for comments on the manuscript; and Lea M. Miller for excellent technical support. This study was supported by National Institute of Neurological Disorders and Stroke of the NIH Grant R37NS008174, the Wayne E. Crill Endowed Professorship.

1. Di Paolo G, De Camilli P (2006) Phosphoinositides in cell regulation and membrane dynamics. *Nature* 443(7112):651–657.
2. Hille B, Dickson EJ, Kruse M, Vivas O, Suh BC (2015) Phosphoinositides regulate ion channels. *Biochim Biophys Acta* 1851(6):844–856.
3. Balla T (2013) Phosphoinositides: Tiny lipids with giant impact on cell regulation. *Physiol Rev* 93(3):1019–1137.
4. Hilgemann DW, Ball R (1996) Regulation of cardiac Na^+,Ca^{2+} exchange and K_{ATP} potassium channels by PIP_2. *Science* 273(5277):956–959.
5. Suh BC, Hille B (2008) PIP_2 is a necessary cofactor for ion channel function: How and why? *Annu Rev Biophys* 37:175–195.
6. Allison JH, Blisner ME, Holland WH, Hipps PP, Sherman WR (1976) Increased brain myo-inositol 1-phosphate in lithium-treated rats. *Biochem Biophys Res Commun* 71(2):664–670.
7. Allison JH, Stewart MA (1971) Reduced brain inositol in lithium-treated rats. *Nat New Biol* 233(43):267–268.
8. Harwood AJ (2005) Lithium and bipolar mood disorder: The inositol-depletion hypothesis revisited. *Mol Psychiatry* 10(1):117–126.
9. Prpić V, Blackmore PF, Exton JH (1982) myo-Inositol uptake and metabolism in isolated rat liver cells. *J Biol Chem* 257(19):11315–11322.
10. Sherman WR, Gish BG, Honchar MP, Munsell LY (1986) Effects of lithium on phosphoinositide metabolism in vivo. *Fed Proc* 45(11):2639–2646.
11. Balla T, Baukal AJ, Guillemette G, Catt KJ (1988) Multiple pathways of inositol polyphosphate metabolism in angiotensin-stimulated adrenal glomerulosa cells. *J Biol Chem* 263(9):4083–4091.
12. Honchar MP, Ackermann KE, Sherman WR (1989) Chronically administered lithium alters neither myo-inositol monophosphatase activity nor phosphoinositide levels in rat brain. *J Neurochem* 53(2):590–594.
13. Jenkinson S, Nahorski SR, Challiss RA (1994) Disruption by lithium of phosphatidylinositol-4,5-bisphosphate supply and inositol-1,4,5-trisphosphate generation in

Chinese hamster ovary cells expressing human recombinant m1 muscarinic receptors. *Mol Pharmacol* 46(6):1138–1148.
14. Berry GT, Buccafusca R, Greer JJ, Eccleston E (2004) Phosphoinositide deficiency due to inositol depletion is not a mechanism of lithium action in brain. *Mol Genet Metab* 82(1):87–92.
15. Malhi GS, Tanious M, Das P, Coulston CM, Berk M (2013) Potential mechanisms of action of lithium in bipolar disorder. Current understanding. *CNS Drugs* 27(2): 135–153.
16. Lykidis A, Jackson PD, Rock CO, Jackowski S (1997) The role of CDP-diacylglycerol synthetase and phosphatidylinositol synthase activity levels in the regulation of cellular phosphatidylinositol content. *J Biol Chem* 272(52):33402–33409.
17. Kwon HM, et al. (1992) Cloning of the cDNa for a Na^+/myo-inositol cotransporter, a hypertonicity stress protein. *J Biol Chem* 267(9):6297–6301.
18. Berry GT, et al. (1995) The human osmoregulatory Na^+/myo-inositol cotransporter gene (SLC5A3): Molecular cloning and localization to chromosome 21. *Genomics* 25(2):507–513.
19. Abramson J, Wright EM (2009) Structure and function of Na^+-symporters with inverted repeats. *Curr Opin Struct Biol* 19(4):425–432.
20. Gamba G (2001) Alternative splicing and diversity of renal transporters. *Am J Physiol Renal Physiol* 281(5):F781–F794.
21. Hager K, et al. (1995) Kinetics and specificity of the renal Na^+/myo-inositol cotransporter expressed in Xenopus oocytes. *J Membr Biol* 143(2):103–113.
22. Battaglia FC, Meschia G, Blechner JN, Barron DH (1961) The free myo-inositol concentration of adult and fetal tissues of several species. *Q J Exp Physiol Cogn Med Sci* 46:188–193.
23. Sigal SH, Yandrasitz JR, Berry GT (1993) Kinetic evidence for compartmentalization of myo-inositol in hepatocytes. *Metabolism* 42(3):395–401.
24. Buccafusca R, et al. (2008) Characterization of the null murine sodium/myo-inositol cotransporter 1 (Smit1 or Slc5a3) phenotype: Myo-inositol rescue is independent of expression of its cognate mitochondrial ribosomal protein subunit 6 (Mrps6) gene and of phosphatidylinositol levels in neonatal brain. *Mol Genet Metab* 95(1–2):81–95.
25. Miyakawa H, Woo SK, Dahl SC, Handler JS, Kwon HM (1999) Tonicity-responsive enhancer binding protein, a rel-like protein that stimulates transcription in response to hypertonicity. *Proc Natl Acad Sci USA* 96(5):2538–2542.
26. Lien YH, Shapiro JI, Chan L (1990) Effects of hypernatremia on organic brain osmoles. *J Clin Invest* 85(5):1427–1435.
27. Yamashita T, et al. (1998) Regulation of Na^+/myo-inositol cotransporter gene expression in hyperglycemic rat hippocampus. *Brain Res Mol Brain Res* 57(1):167–172.
28. Berry GT, Wang ZJ, Dreha SF, Finucane BM, Zimmerman RA (1999) In vivo brain myo-inositol levels in children with Down syndrome. *J Pediatr* 135(1):94–97.
29. Miller BL, et al. (1993) Alzheimer disease: Depiction of increased cerebral myo-inositol with proton MR spectroscopy. *Radiology* 187(2):433–437.
30. Watanabe T, Shiino A, Akiguchi I (2012) Hippocampal metabolites and memory performances in patients with amnestic mild cognitive impairment and Alzheimer's disease. *Neurobiol Learn Mem* 97(3):289–293.
31. Bitsch A, et al. (1999) Inflammatory CNS demyelination: Histopathologic correlation with in vivo quantitative proton MR spectroscopy. *AJNR Am J Neuroradiol* 20(9): 1619–1627.
32. Castillo M, Smith JK, Kwock L (2000) Correlation of myo-inositol levels and grading of cerebral astrocytomas. *AJNR Am J Neuroradiol* 21(9):1645–1649.
33. Huang W, et al. (1999) High brain myo-inositol levels in the predementia phase of Alzheimer's disease in adults with Down's syndrome: A 1H MRS study. *Am J Psychiatry* 156(12):1879–1886.
34. Patel NC, et al. (2006) Lithium treatment effects on Myo-inositol in adolescents with bipolar depression. *Biol Psychiatry* 60(9):998–1004.
35. Abbott GW, et al. (2014) KCNQ1, KCNE2, and Na^+-coupled solute transporters form reciprocally regulating complexes that affect neuronal excitability. *Sci Signal* 7(315): ra22.
36. Telezhkin V, Brown DA, Gibb AJ (2012) Distinct subunit contributions to the activation of M-type potassium channels by $PI(4,5)P_2$. *J Gen Physiol* 140(1):41–53.
37. Suh BC, Hille B (2002) Recovery from muscarinic modulation of M current channels requires phosphatidylinositol 4,5-bisphosphate synthesis. *Neuron* 35(3):507–520.
38. Brown DA, Marrion NV, Smart TG (1989) On the transduction mechanism for muscarine-induced inhibition of M-current in cultured rat sympathetic neurones. *J Physiol* 413:469–488.
39. Szentpetery Z, Balla A, Kim YJ, Lemmon MA, Balla T (2009) Live cell imaging with protein domains capable of recognizing phosphatidylinositol 4,5-bisphosphate; a comparative study. *BMC Cell Biol* 10:67.
40. Santagata S, et al. (2001) G-protein signaling through tubby proteins. *Science* 292(5524):2041–2050.
41. Hammond GR, et al. (2012) PI4P and $PI(4,5)P_2$ are essential but independent lipid determinants of membrane identity. *Science* 337(6095):727–730.
42. Hammond GR, Machner MP, Balla T (2014) A novel probe for phosphatidylinositol 4-phosphate reveals multiple pools beyond the Golgi. *J Cell Biol* 205(1):113–126.
43. Dickson EJ, Jensen JB, Hille B (2014) Golgi and plasma membrane pools of PI(4)P contribute to plasma membrane $PI(4,5)P_2$ and maintenance of KCNQ2/3 ion channel current. *Proc Natl Acad Sci USA* 111(22):E2281–E2290.
44. Szentpetery Z, Várnai P, Balla T (2010) Acute manipulation of Golgi phosphoinositides to assess their importance in cellular trafficking and signaling. *Proc Natl Acad Sci USA* 107(18):8225–8230.
45. Wenk MR (2005) The emerging field of lipidomics. *Nat Rev Drug Discov* 4(7):594–610.
46. Clark J, et al. (2011) Quantification of $PtdInsP_3$ molecular species in cells and tissues by mass spectrometry. *Nat Methods* 8(3):267–272.
47. Berridge MJ (1998) Neuronal calcium signaling. *Neuron* 21(1):13–26.
48. Clapham DE (2007) Calcium signaling. *Cell* 131(6):1047–1058.
49. Tanimura A, Nezu A, Morita T, Turner RJ, Tojyo Y (2004) Fluorescent biosensor for quantitative real-time measurements of inositol 1,4,5-trisphosphate in single living cells. *J Biol Chem* 279(37):38095–38098.
50. Dickson EJ, Falkenburger BH, Hille B (2013) Quantitative properties and receptor reserve of the IP_3 and calcium branch of G_q-coupled receptor signaling. *J Gen Physiol* 141(5):521–535.
51. Logothetis DE, Kurachi Y, Galper J, Neer EJ, Clapham DE (1987) The $\beta\ \gamma$ subunits of GTP-binding proteins activate the muscarinic K^+ channel in heart. *Nature* 325(6102): 321–326.
52. Whorton MR, MacKinnon R (2011) Crystal structure of the mammalian GIRK2 K^+ channel and gating regulation by G proteins, PIP_2, and sodium. *Cell* 147(1):199–208.
53. Kobrinsky E, Mirshahi T, Zhang H, Jin T, Logothetis DE (2000) Receptor-mediated hydrolysis of plasma membrane messenger PIP_2 leads to K^+-current desensitization. *Nat Cell Biol* 2(8):507–514.
54. Runnels LW, Yue L, Clapham DE (2002) The TRPM7 channel is inactivated by PIP_2 hydrolysis. *Nat Cell Biol* 4(5):329–336.
55. Bissonnette P, Lahjouji K, Coady MJ, Lapointe JY (2008) Effects of hyperosmolarity on the Na^+ -myo-inositol cotransporter SMIT2 stably transfected in the Madin-Darby canine kidney cell line. *Am J Physiol Cell Physiol* 295(3):C791–C799.
56. Kino T, et al. (2009) Brx mediates the response of lymphocytes to osmotic stress through the activation of NFAT5. *Sci Signal* 2(57):ra5.
57. Kwon HM, Handler JS (1995) Cell volume regulated transporters of compatible osmolytes. *Curr Opin Cell Biol* 7(4):465–471.
58. Rao A, Luo C, Hogan PG (1997) Transcription factors of the NFAT family: Regulation and function. *Annu Rev Immunol* 15:707–747.
59. Woo SK, Maouyo D, Handler JS, Kwon HM (2000) Nuclear redistribution of tonicity-responsive enhancer binding protein requires proteasome activity. *Am J Physiol Cell Physiol* 278(2):C323–C330.
60. Lammers PE, Beck JA, Chu S, Kempson SA (2005) Hypertonic upregulation of betaine transport in renal cells is blocked by a proteasome inhibitor. *Cell Biochem Funct* 23(5): 315–324.
61. Kim YJ, Guzman-Hernandez ML, Wisniewski E, Balla T (2015) Phosphatidylinositol-phosphatidic acid exchange by Nir2 at ER-PM contact sites maintains phosphoinositide signaling competence. *Dev Cell* 33(5):549–561.
62. Suh BC, Hille B (2007) Electrostatic interaction of internal Mg^{2+} with membrane PIP_2 seen with KCNQ K^+ channels. *J Gen Physiol* 130(3):241–256.
63. Zhang Q, et al. (2013) Dynamic PIP_2 interactions with voltage sensor elements contribute to KCNQ2 channel gating. *Proc Natl Acad Sci USA* 110(50):20093–20098.
64. Kim KS, Duignan KM, Hawryluk JM, Soh H, Tzingounis AV (2016) The voltage activation of cortical KCNQ channels depends on global PIP_2 levels. *Biophys J* 110(5): 1089–1098.
65. Shapiro MS, et al. (2000) Reconstitution of muscarinic modulation of the KCNQ2/KCNQ3 K^+ channels that underlie the neuronal M current. *J Neurosci* 20(5):1710–1721.
66. Sardini A, et al. (2003) Cell volume regulation and swelling-activated chloride channels. *Biochim Biophys Acta* 1618(2):153–162.
67. Almaça J, et al. (2009) TMEM16 proteins produce volume-regulated chloride currents that are reduced in mice lacking TMEM16A. *J Biol Chem* 284(42):28571–28578.
68. Voss FK, et al. (2014) Identification of LRRC8 heteromers as an essential component of the volume-regulated anion channel VRAC. *Science* 344(6184):634–638.
69. Qiu Z, et al. (2014) SWELL1, a plasma membrane protein, is an essential component of volume-regulated anion channel. *Cell* 157(2):447–458.
70. Grunnet M, et al. (2003) KCNQ1 channels sense small changes in cell volume. *J Physiol* 549(Pt 2):419–427.
71. Bessac BF, Fleig A (2007) TRPM7 channel is sensitive to osmotic gradients in human kidney cells. *J Physiol* 582(Pt 3):1073–1086.
72. Prager-Khoutorsky M, Khoutorsky A, Bourque CW (2014) Unique interweaved microtubule scaffold mediates osmosensory transduction via physical interaction with TRPV1. *Neuron* 83(4):866–878.
73. Nasuhoglu C, et al. (2002) Modulation of cardiac PIP_2 by cardioactive hormones and other physiologically relevant interventions. *Am J Physiol Cell Physiol* 283(1): C223–C234.
74. Yamamoto M, et al. (2006) Hypertonic stress increases phosphatidylinositol 4,5-bisphosphate levels by activating PIP5KIbeta. *J Biol Chem* 281(43):32630–32638.
75. Zhang Z, Ferraris JD, Brooks HL, Brisc I, Burg MB (2003) Expression of osmotic stress-related genes in tissues of normal and hyposmotic rats. *Am J Physiol Renal Physiol* 285(4):F688–F693.
76. Vivas O, Kruse M, Hille B (2014) Nerve growth factor sensitizes adult sympathetic neurons to the proinflammatory peptide bradykinin. *J Neurosci* 34(36):11959–11971.
77. Falkenburger BH, Jensen JB, Hille B (2010) Kinetics of PIP_2 metabolism and KCNQ2/3 channel regulation studied with a voltage-sensitive phosphatase in living cells. *J Gen Physiol* 135(2):99–114.